Study of the $^{13}N(d,n)^{14}O$ reaction cross section and its astrophysical implications for the ^{13}N proton capture reaction

P. Decrock, M. Gaelens, M. Huyse, G. Reusen, G. Vancraeynest, P. Van Duppen, and J. Wauters
Instituut voor Kern-en Stralingsfysika, Katholieke Universiteit Leuven, Leuven, Belgium

Th. Delbar, W. Galster, P. Leleux, I. Licot, E. Liénard, P. Lipnik, C. Michotte, and J. Vervier
Institut de Physique Nucléaire, Université Catholique de Louvain, Louvain-la-Neuve, Belgium

H. Oberhummer
Institute of Nuclear Physics, Technical University Wien, Wien, Austria
(Received 19 April 1993)

The total cross section for the $^{13}N(d,n)^{14}O_{g.s.}$ reaction has been measured with ^{13}N radioactive beams at laboratory energies of 8.2, 12.0, 16.2, and 28.5 MeV. A spectroscopic factor of 0.9 is obtained from a distorted-wave Born approximation analysis of this transfer reaction. The astrophysical S factor for the $^{13}N(p,\gamma)^{14}O$ reaction is calculated using the experimentally known resonance parameters for the resonant contribution and the direct-capture model with the experimental spectroscopic factor for the nonresonant contribution.

PACS number(s): 25.45.Hi, 25.40.Lw, 95.30.Cq

I. INTRODUCTION

Recently we reported on a measurement of the integrated cross section of the $^{13}N(p,\gamma)^{14}O$ radiative capture reaction in the energy range of the 0.526 MeV, 1^- resonance [1]. In addition to the pure Breit-Wigner resonant contribution, the total cross section for this reaction contains a nonresonant direct-capture contribution in which case the $E1$ transition proceeds without formation of an intermediate resonant state [2]. Moreover, the tails of the resonance are significantly influenced by the interference effect between the resonant and nonresonant amplitudes [2]. A precise knowledge of the $^{13}N(p,\gamma)^{14}O$ reaction cross section, especially of the low-energy tail of the resonance (the Gamow peak energy amounts to 93 keV for a stellar temperature of 10^8 K), is important as it plays a key role in the hot carbon-nitrogen-oxygen (CNO) cycle [3] where, due to the high temperatures ($\geq 10^8$ K), the proton capture rate by ^{13}N can become of the same order or larger than the ^{13}N decay rate. The calculation of this nonresonant cross section requires the knowledge of the spectroscopic factor for the $^{13}N(d,n)^{14}O_{g.s.}$ reaction, which contains the nuclear structure information and is related to the probability for finding the ^{14}O ground-state wave function in the configuration formed by the ^{13}N ground-state wave function with $J^\pi=\frac{1}{2}^-$ coupled to a proton in the $l_p=1(p1/2)$ shell-model orbit. Since the introduction of the distorted-wave Born approximation (DWBA) stripping theory, many single-particle transfer reactions [of the types (d,n), (d,p), $(^3He,d)$, etc.] on light nuclei have been studied in order to obtain spectroscopic information about these nuclei in particular, to determine spectroscopic factors.

In this work, we present the results of total cross-section determinations of the proton-transfer reaction $^2H(^{13}N,n)^{14}O$, measured at different energies by using ^{13}N beams. With the Belgian Radioactive Ion Beam facility [4], energetic and intense radioactive nuclear beams are presently available making possible these types of measurements. In Sec. II, the experimental setup, the typical problems related to the use of high-intensity radioactive nuclear beams, the uncertainties concerning the absolute normalization of the measurement (detection efficiency, target thickness, stopping power, elastic scattering), and finally the results of the cross-section measurements are discussed. Section III deals with the data analysis of the measured $^{13}N(d,n)^{14}O_{g.s.}$ excitation function in the framework of a potential model (DWBA) [5]. This excitation function is also compared with $^{14}N(d,n)^{15}O_{g.s.}$ and $^{13}C(d,n)^{14}N_{g.s.}$ excitation functions taken from the literature. Finally, in Sec. IV, a calculation of the $^{13}N(p,\gamma)^{14}O$ astrophysical S factor, in the 0–1000 keV region, is presented, based on the formalism proposed by Rolfs and co-workers [2,3], which includes a resonant, a nonresonant, and an interference term. For the nuclear input parameters (resonance energy and gamma and proton widths), the experimental values obtained with ^{13}N beams [1,6] have been used. With the obtained astrophysical S factor, the thermonuclear reaction rate has been calculated.

II. MEASUREMENT OF THE $^{13}N(d,n)^{14}O_{g.s.}$ TOTAL REACTION CROSS SECTION

A. Experimental setup

The $^{13}N(d,n)^{14}O$ cross section has been measured at four ^{13}N laboratory energies (8.2, 12.0, 16.2, and 28.5

MeV) by using a radioactive $^{13}N(T_{1/2}=9.96$ m) beam; these beam energies correspond to 1.0, 1.5, 2.0, and 3.8 MeV, respectively, in the center-of-mass system. The ^{13}N beam was delivered by the Belgian Radioactive Ion Beam facility [4], with intensities varying from $\simeq 5$ particles pA (at 12.0, 16.2, and 28.5 MeV) to $\simeq 15$ particles pA (at 8.2 MeV). A schematical drawing of the detection setup is shown in Fig. 1. The ^{13}N beam was sent on a deuterated polyethylene target $(CD_2)_n$ which was mounted in the reaction chamber. Different $(CD_2)_n$ foils were used with thicknesses varying between 50 and 300 $\mu g/cm^2$. The $(CD_2)_n$ target was positioned in front of an aluminized Mylar tape (which has a width of 12.8 mm) at a distance ≤ 5 mm. The ^{13}N beam particles and the ^{14}O reaction products were implanted in the catcher tape, which, after an implantation time of 128 s, was moved to a decay station, where the produced ^{14}O ($T_{1/2}=70.59$ s) nuclei were detected through the delayed 2.3 MeV γ ray (absolute branching of 99.39%) following the β^+ decay of ^{14}O. Note that, due to the reverse kinematics, the ^{14}O nuclei have a maximum scattering angle that, depending on the energy, lies for our measurements between 7.8° and 10.9°; this means that all ^{14}O particles are implanted in the tape. In the reaction chamber, two silicon detectors were mounted which recorded the scattered ^{13}N and the recoiling deuterons. In order to detect these scattered particles, the target was pulled backwards with respect to the tape; by changing the distance between the target and implantation tape from 30 to 70 mm, a scattering angle between 33° and 15° could be chosen. Gamma rays and particles have been detected in separated runs.

B. γ-ray detection

1. Detection of the 2.3 MeV γ ray in a high β^+-radiation environment

The γ detection was carried out with two large volume Ge detectors (70% and 90% efficiencies on the 1332 keV γ line of ^{60}Co relative to a 7.6 cm×7.6 cm NaI at a source to detector distance of 25 cm). In order to reduce the contribution of the annihilation radiation from the β^+ decaying ^{13}N atoms, 3–4 cm of lead was inserted between the source and the detectors. Furthermore, the detectors were placed in a cylindrical lead shielding with a wall thickness of 10 cm in order to reduce the ambient background. Between this cylindrical Pb shielding and the detectors, a Cu and Sn shielding was also placed in order to reduce the Pb x rays.

Time sequential single spectra, with four counting periods of 32 seconds each, have been recorded for the gamma detection. Figure 2 shows parts of the γ spectra between 1.8 and 2.8 MeV summed over the four time units. The 2.313 MeV γ line from the decay of ^{14}O is clearly observed, together with two background lines coming from natural radioactivity, the line at 2.615 MeV with its first escape peak at 2.104 MeV, and the line at 2.204 MeV, originating from the ^{232}Th and ^{238}U decay chains, respectively. The line at 2.168 MeV, clearly seen in the spectrum registered at an incident energy of 28.5 MeV, is due to the β^+ decay of ^{38}K produced in the aluminized Mylar tape by the $^{27}Al(^{13}N,pn)^{38}K$ reaction. The time behavior of the intensity of the observed 2.313 MeV γ line, which supports its assignment to the decay of ^{14}O, is shown in Fig. 3, where the curves are fits with a fixed 70.59 s half live. Figure 4 shows, as an example, the total γ spectrum registered, with the 70% detector, during the first time unit at a beam energy of 28.5 MeV:

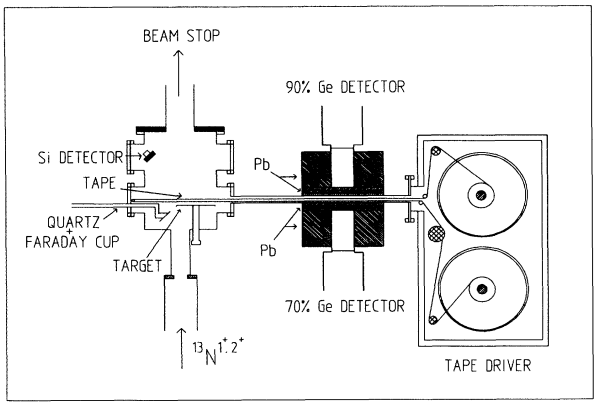

FIG. 1. Experimental setup used in the present experiment, including the reaction chamber with the $(CD_2)_n$ target and the particle detectors, the tape system and the lead-shielded Ge detectors.

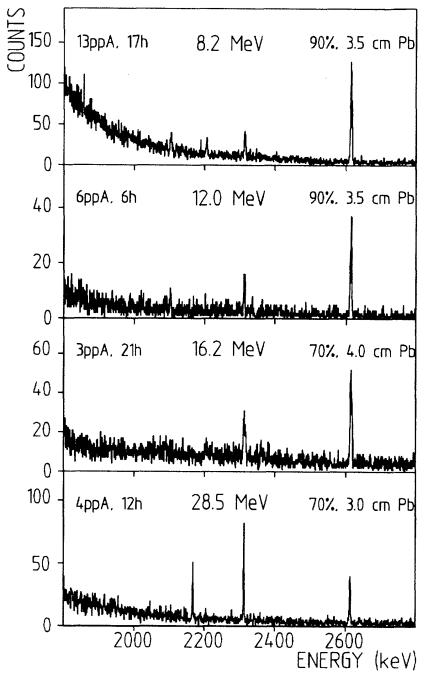

FIG. 2. γ-ray energy spectra between 1.8 and 2.8 MeV registered with one of the two germanium detectors (70% or 90%) at ^{13}N beam energies of 8.2, 12.0, 16.2, and 28.5 MeV. The line at 2.3 MeV following the decay of ^{14}O is clearly shown. The thickness of the lead shielding between source and detector, the average ^{13}N beam intensity (in particles pA) and the measuring time (in hours), are quoted.

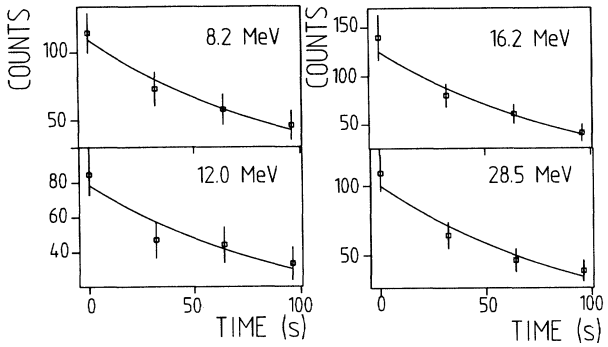

FIG. 3. Fits, with a constant half-life of 70.59 s (^{14}O), of the experimental 2.3 MeV γ-ray intensities as function of time, suggesting the assignment of the 2.3 MeV γ line to the decay of ^{14}O.

it is dominated by the 0.511 MeV γ line, by the bremsstrahlung arising from the stopping of the positrons in the lead shielding (the β^+ end-point energy of ^{13}N is 1.2 MeV), and by its summing with the 0.511 MeV line. The peak present at the end of the spectrum arises from a pulse generator. It is clear from Figs. 2 and 4 that the limitation of this method, namely, the γ-ray detection in an environment of a highly intense β^+ source (coming from the radioactive ion beam itself), is the β^+ end-point energy of the radioactive ion beam.

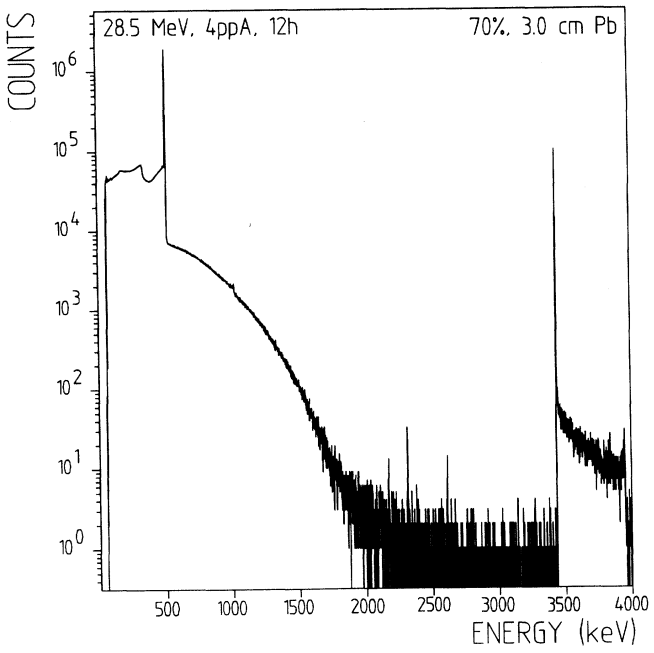

FIG. 4. Example of a total γ-ray spectrum (registered during the first time unit) showing the dominance of the 0.511 MeV line and of the bremsstrahlung due to the stopping of the β^+ particles of ^{13}N. The line at the end of the spectrum arises from a pulse generator. For this spectrum, the average count rate was 3100 counts/s; the pulser line yields an estimate for the pile up of 12.8%.

2. *Detection efficiency*

The intensities of the gamma lines have been corrected for dead-time and pile up effects. These corrections, which vary between 1% and 15% depending on the ^{13}N beam intensity and the lead shielding, are determined on-line with a pulse generator. The γ-ray efficiencies of the two germanium detectors were measured in the experimental position by using a ^{56}Co source and intensity-calibrated sources of ^{60}Co, ^{152}Eu, ^{137}Cs, and ^{22}Na, which cover an energy range between 0.511 and 3.5 MeV. As an example, the detection efficiency as a function of energy for the 70% detector in the case of a lead shielding of 4 cm is shown in Fig. 5; note that the 0.511 MeV efficiency is suppressed by a factor of 36 relative to the 2.3 MeV efficiency. The total detection efficiency (70%+90% detectors) for the 2.3 MeV γ line lies between 1.6×10^{-3} (4 cm Pb 70% and 4 cm Pb 90% detector) and 3.0×10^{-3} (3 cm Pb 70% and 3.5 cm Pb 90%).

C. Data normalization and results

1. *Determination of the cross section*

The $^{13}N(d,n)^{14}O$ absolute cross section is derived in two different ways. The first method uses the well-known relation between the reaction yield Y and the cross section σ (in units of cm^2) [3]:

$$\sigma = Y/(\eta \Delta X) , \tag{1}$$

where η is the number of active target nuclei per cm^3, ΔX is the target thickness in cm and Y is the reaction yield, i.e., the number of reactions per incoming projectile. In

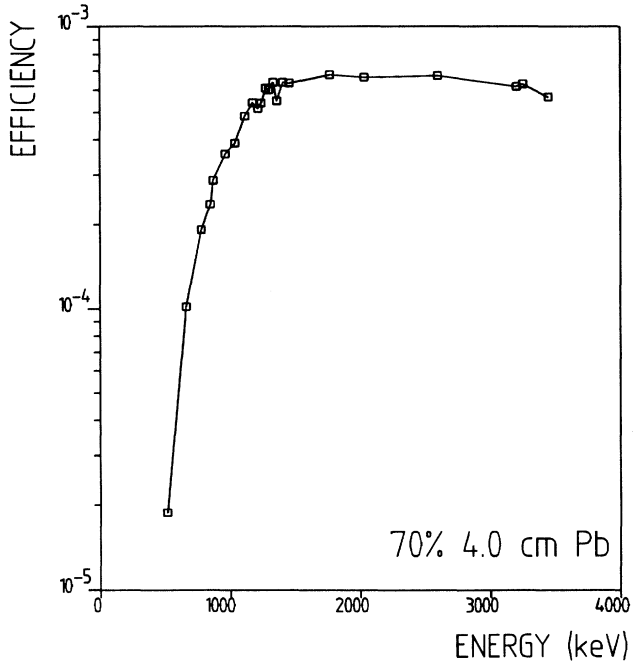

FIG. 5. γ-ray detection efficiency for the 70% Ge detector shielded with 4 cm of lead.

the case of $^{13}N(d,n)^{14}O$, the reaction yield can be deduced, after straightforward corrections for efficiency and half-life, from the ratio between the number of γ rays at 2.3 MeV and the number of annihilation radiations at 0.511 MeV. Since Y depends on the ratio between two γ-ray intensities, the dead-time and pile up corrections cancel in this method. For the case of a $(CD_2)_n$ target, relation (1) can be rewritten as follows:

$$\sigma = Y/(8N_A T) , \tag{2}$$

where N_A is the Avogadro number and T is the target thickness expressed in g/cm^2. The determination of T, which is important for the normalization with this first method, is discussed in Sec. II C 2.

In the second method, one compares, for an equal number of 0.511 MeV counts (i.e., for the same integrated beam current), the number of 2.3 MeV γ counts with the number of elastically scattered deuterons registered in the silicon detector mounted in the reaction chamber.

$$\sigma = \frac{I_\gamma}{I_{\text{deuteron}}} \left[\frac{d\sigma}{d\omega} \right]_{\text{lab}} d\omega , \tag{3}$$

where I_γ is the 2.3 MeV γ intensity corrected for efficiency and losses due to the implantation and decay sequence, I_{deuteron} is the number of elastically scattered deuterons in the solid angle $d\omega$ of the silicon detector, and $(d\sigma/d\omega)_{\text{lab}}$ is the average value, in the target, of the differential Rutherford cross section in the laboratory system. The assumption of a pure Rutherford cross section for elastic scattering is valid only when the reaction occurs below the Coulomb barrier; for our measurements, this is only valid for the three measurements at the lowest beam energies. As the fourth measurement at 3.8 MeV (center of mass) is above the Coulomb barrier, only the first method of normalization has been used in this case. The main advantage of this second method is that the data normalization is independent of the target thickness (i.e., stopping power) and of the target composition. With the second method, however, another uncertainty is involved, namely, the uncertainty on the beam position on the target, which influences the scattering angle and thereby the elastic cross section.

2. *Target thickness*

The thickness T (in g/cm^2) of the $(CD_2)_n$ targets can be deduced from the energy loss ΔE of the ^{13}N beam in the target (expressed in MeV) through the relation:

$$T = \Delta E / S , \tag{4}$$

where S is the stopping power of the ^{13}N beam in the target, expressed in MeV/(g/cm^2). A more intense ^{13}C beam, and its corresponding stopping power S, can also be used for determining the target thickness T.

The energy loss ΔE can be obtained from fits to the elastically scattered deuteron peak in the particle spectrum. As an example, Fig. 6 shows parts of two-particle spectra (at $\theta_{\text{lab}} = 32.9°$), registered with a ^{13}C beam of 12.0 MeV and two different target thicknesses: the difference in foil thickness is reflected by the difference

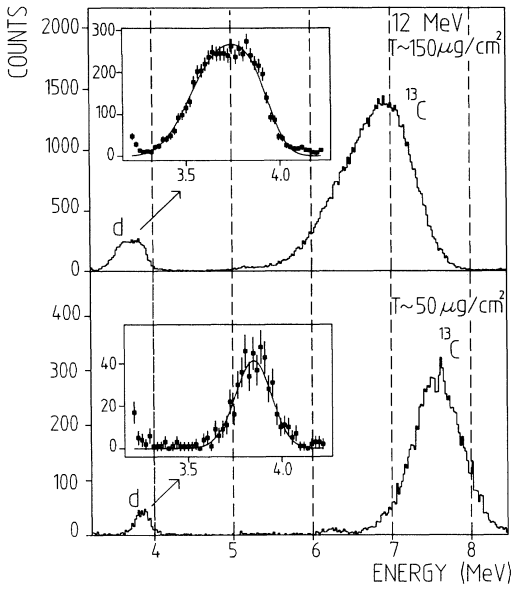

FIG. 6. Parts of the particle spectra obtained with a ^{13}C incident beam and two different $(CD_2)_n$ target thicknesses, showing the elastically scattered ^{13}C particles and the recoiling deuterons. The insets show the fits to the deuteron peaks described in the text.

between the energies at which the ^{13}C peak is observed, and by the broadening of the deuteron peak. The insets show fits to the deuteron peaks. These fits not only reveal information on the incoming and outgoing energies of the beam (and thus on ΔE), but also on the energy resolution of the incoming and outgoing beam; this information is reflected by the high-energy (incoming beam) and low-energy (outgoing beam) sides of the scattered deuteron peaks. The energy resolution of the incoming beam, which depends on the cyclotron performances, lies in the best case around 150 keV. When the beam travels through the target, its energy width increases due to the target inhomogeneity and to energy-loss straggling. This creates an asymmetric deuteron peak, i.e., a broader energy spread on the low-energy side compared to the high-energy side. A typical value for the additional energy spread of the outgoing beam due to this effect (which has to be added quadratically to the beam resolution itself) is of the order of 150 keV for a beam energy loss of about 1 MeV in the target: this shows that the polyethylene $(CD_2)_n$ targets have reasonably good qualities.

The effective stopping power S [in MeV/(g/cm^2)] of ^{13}N and ^{13}C in CD_2 can be taken from the calculations of Ziegler [7], which show that, within a typical energy loss of 1 MeV in the target, the stopping power remains approximately constant. This is confirmed by the tables of Northcliffe and Schilling [8]. However, there are significant differences between the absolute stopping powers given by the two tables, as shown in Table I where the stopping powers for ^{13}N and ^{13}C from both references are compared: differences of the order of 20% are observed.

The target thickness T can also be determined by

TABLE I. Comparison between the stopping powers S [in meV/(mg/cm^2)] for ^{13}C, ^{13}N ions, and α particles in $(CD_2)_n$ foils given by Ziegler [7] and by Northcliffe and Schilling [8].

S [MeV/(mg/cm^2)]	^{13}C 8.2 MeV	^{13}C 12.0 MeV	^{13}N 16.2 MeV	α 5.5 MeV
Reference [7]	7.4	6.6	7.4	0.82
Reference [8]	9.3	8.1	8.9	0.93

measuring the energy loss of an α particle passing through the target, using relation (4). Figure 7 shows the energy shifts of the three α lines at 5.15, 5.48, and 5.80 MeV, arising from a mixed ^{239}Pu, ^{241}Am, and ^{244}Cm α source, after passing through two $(CD_2)_n$ foils of different thicknesses. The stopping powers of the α particles in CD_2 can again be taken from the tables of Ziegler [7] or of Northcliffe and Schilling [8]. Table I shows that the difference between the absolute stopping powers for the α particles in the two references is about 10%.

Concerning the data normalization, one should note that the polyethylene targets also contain a small amount of hydrogen. This amount lies around 5% compared to the deuteron content, and is determined from the ratio between the numbers of elastic-scattered protons and deuterons in the particle detector.

3. *Results*

The normalization of the cross section at the lowest three energies (8.2, 12.0, and 16.3 MeV) has been performed by using the two methods described in Sec. II C 1. Since the cross sections obtained at the same energy with targets of different thicknesses are equal to within 15%, the average value is adopted. The results of the total cross-section measurements with the different normalization methods are shown in Fig. 8; the squares and triangles correspond to the use of the Ziegler [7] and Northcliffe and Schilling [8] stopping powers, respectively. The target thickness has been determined with a ^{13}C beam for the measurements at 8.2 and 12.0 MeV, and with the ^{13}N beam itself for the measurement at 16.2 MeV. One can also observe that the cross section normalized with the second method (circles in Fig. 8), which is independent on the target thickness, lies between the results obtained with the first method by using the two stopping power tables. For the further analysis of the results (Sec. III), an average value for the cross sections is adopted, which approximately corresponds (for the lowest three energies) to the results obtained using the second normalization method. From these considerations, an uncertainty of about 20% should be adopted for the absolute values of the average cross sections.

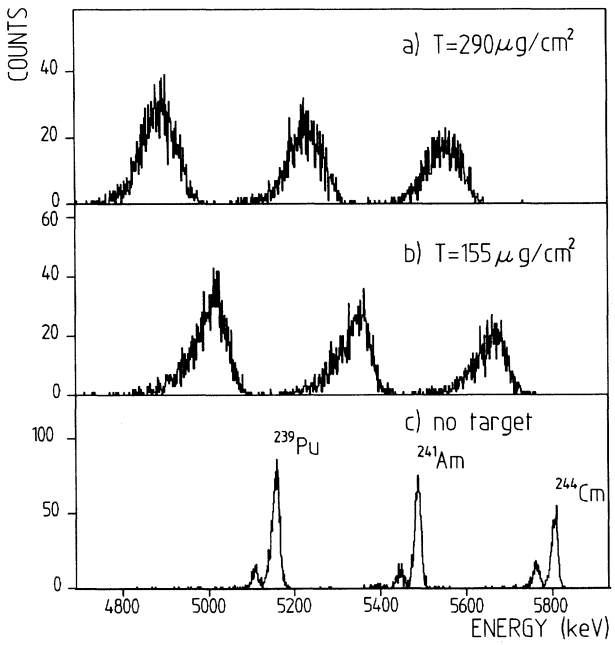

FIG. 7. Energy shift of the three alpha lines (5.15, 5.48, and 5.8 MeV) when passing through $(CD_2)_n$ targets of different thicknesses: (a) $T=290$ μg/cm^2; (b) $T=155$ μg/cm^2; (c) no target.

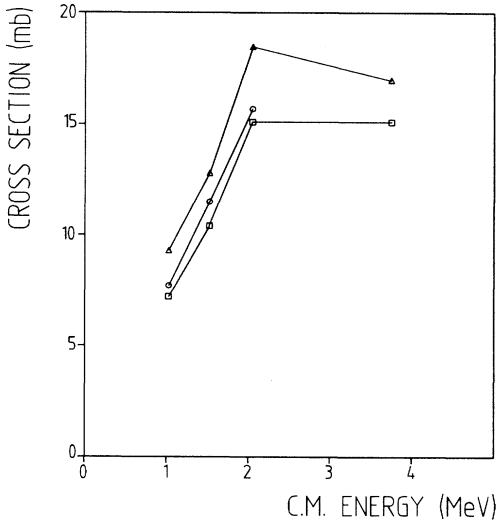

FIG. 8. Experimental cross sections for the $^{13}N(d,n)^{14}O_{g.s.}$ reaction measured at four energies. The different cross sections for each energy correspond to the different normalization methods: the circles, to the elastic-scattering normalization method; the squares and the triangles, to a normalization using the stopping powers of Ziegler [7] and Northcliffe and Schilling [8], respectively.

III. DETERMINATION OF THE SPECTROSCOPIC FACTOR

A. DWBA formalism

For the analysis of the measured total cross section for the $^{13}N(d,n)^{14}O_{g.s.}$ reaction, a potential-model calculation has been used, the distorted-wave Born approximation (DWBA). A detailed study of the differential cross sections and of the reaction mechanism for $l_p=1$ stripping processes on nuclei in the $1p$ shell, for center-of-mass energies in the 1–3 MeV range, has been presented by Siemssen, Cosack, and Felst [9]. They have compared the differential (d,n) stripping cross sections on various light nuclei (^{6}Li, ^{9}Be, ^{10}B, ^{11}B, ^{12}C, and ^{14}N) and found a striking similarity in the variation of the overall shape of these angular distributions with energy, a fact which can be interpreted as a direct-interaction (DI) phenomenon. In addition, the total cross sections as functions of energy (yield curves) show no strong fluctuations, suggesting that the compound amplitude is small. The general way to determine spectroscopic factors from transfer reaction data is by comparing the experimental differential cross sections with theoretical DWBA calculations; in some cases, a compound-nucleus contribution is incoherently added to the direct-interaction cross section [10,11].

For the stripping calculations, we have used the DWBA computer program FREDICA [12]. The general expression of the differential cross section for the transfer reaction $a+A\rightarrow b+B$ with $a-x=b$ and $A+x=B$ is given, in zero-range DWBA, by [5]

$$\left[\frac{d\sigma}{d\Omega}\right]^{\mathrm{DWBA}}=\left[\frac{4\pi^2\mu^\alpha\mu^\beta k^\beta}{h^4k^\alpha}\frac{2I_B+1}{2I_A+1}\right]\times\sum_{lsj}C^2S_{lj}N|T_{lsj}^{\mathrm{DWBA}}|^2/(2s+1)\ . \tag{5}$$

In this equation, μ^α and μ^β and k^α and k^β are the reduced masses μ and wave numbers k in the entrance channel α and exit channel β, respectively. I_A and I_B are the spins of the target and residual nuclei, respectively. The orbital angular momentum number l, the spin quantum number s, and the total angular momentum j refer to the transferred nucleon x (in our case, the transferred proton), which is bound in the residual nucleus B. The zero-range normalization constant is given by N ($N=aD_0^2/2$ with $D_0^2=1.65\times10^4$ MeV^2 fm^3). The quantities C and S_{ij} correspond to the isospin Clebsch-Gordan coefficient and the spectroscopic factor, respectively. The DWBA-transition amplitude for a specific transfer with orbital, spin, and total angular momentum l, s, and j is given by T_{lsj}^{DWBA} [5]. The total cross section is obtained by integrating the differential cross section over all scattering angles. In Ref. [5], a few examples of DWBA calculations using the code FREDICA, and their comparison with experiment, can be found. The good agreement of these calculations with experiment is explained by the fact that the reactions took place at sub-Coulomb energies where the description with DWBA (DI) is adequate, because at these energies the coupling of the entrance and exit channel to the closed channels is small.

The optical potentials for the entrance and exit channels used in this work have been parametrized as follows:

$$U_{\mathrm{opt}}(r)=V_C(r)-V_{\mathrm{FOLD}}(r)-iWg(r,R,a)+2(\sigma\cdot\mathbf{l})V_{\mathrm{so}}r^{-1}df(r,R_{\mathrm{so}},a_{\mathrm{so}})/dr\ , \tag{6}$$

where g is the derivative of the Woods-Saxon form factor f:

$$g(r,R,a)=4a\,df(r,R,a)/dr$$

with

$$f(r,R,a)=1+\exp[(r-R)/a]^{-1}$$

and

$$R=r_0A^{1/3}\ .$$

In Eq. (6), V_C is the Coulomb potential of a homogeneous sphere with radius $R=r_CA^{1/3}$ with $r_C=1.25$ fm; V_{FOLD} is the nuclear potential; W is the imaginary potential; the fourth term is the spin-orbit contribution (Thomas form).

B. Results and discussion of the DWBA calculations

The real part V_{FOLD} of the potential U_{opt}, which is important for calculating the wave functions of the scattering (entrance and exit channels) and bound states, is determined by using a folding procedure [5,12]. In this approach, the number of free parameters is considerably reduced as compared with more phenomenological potentials (e.g., Woods-Saxon potentials). The nuclear densities are taken from nuclear charge distributions [13] and folded with an energy- and density-dependent nucleon-nucleon (V_{NN}) interaction [14]:

$$V_{\mathrm{FOLD}}(r)=\int\int\rho_A(\mathbf{r}_A)\rho_a(\mathbf{r}_a)V_{NN}\times(E,\rho_A,\rho_a,s=|\mathbf{r}+\mathbf{r}_a-\mathbf{r}_A|)d\mathbf{r}_Ad\mathbf{r}_a\ . \tag{7}$$

The quantity s is the separation between the center of mass of the two colliding nuclei, and ρ_a and ρ_A are the respective nucleon densities. For the bound state, a folding procedure is also used, and the depth of the potential is adjusted to reproduce the experimental proton binding energy.

For the imaginary part [third term in Eq. (6)], a potential of the Woods-Saxon (surface) type is used. For the Woods-Saxon potential parameters, the average parameter sets given in Ref. [15] for deuterons and neutrons have been taken as starting values. The $^{14}N(d,n)^{15}O_{g.s.}$ and $^{13}C(d,n)^{14}N^*$ (2.31 MeV) total and differential reaction cross sections have then been calculated and compared with experimental data. In order to improve the reproduction of the experimental differential cross section of the above-mentioned reactions, the imaginary parts of the optical parameters in the DWBA calculation have been slightly modified as compared to Ref. [15]. We have added a spin-orbit term, which improved the agreement at backward angles. The following parameters have been used: for the entrance channel (deuteron), $W=-16$

MeV, $r_0=1.34$ fm, and $a=0.68$ fm and $V_{so}=-12.0$ MeV, $r_0=1.3$ fm, and $a_{so}=0.5$ fm; and for the exit channel (neutron), $W=-4.0$ MeV, $r_0=1.2$ fm, and $a=0.5$ fm and $V_{so}=-5.5$ MeV, $r_0=1.15$ fm, and $a_{so}=0.57$ fm. The addition of a spin-orbit term improves the differential cross section at backward angles, but the total cross section remains the same since the backward angle cross sections do not significantly contribute to the total cross section.

The spectroscopic factors for $^{14}N(d,n)^{15}O_{g.s.}$ and $^{13}C(d,n)^{14}N^*$ (2.31 MeV) reactions are first obtained out of the comparison (χ^2 test) of the calculated cross sections with the experimental data taken from literature. Then, the $^{13}N(d,n)^{14}O$ total reaction cross section is calculated, using the same optical potential parametrization, and compared with the presently measured cross sections. The results of the calculations of these three (d,n) stripping reactions can be summarized as follows:

1. The $^{14}N(d,n)^{15}O$ reaction

The experimental total cross section for the $^{14}N(d,n)^{15}O_{g.s.}$ reaction obtained by Retz-Schmidt and Weil [16], together with the DWBA calculation, is shown in Fig. 9. The potential parameters used in this calculation are those which are mentioned above. The calculation satisfactorily reproduces the energy dependency of the cross sections, namely, the penetration of the Coulomb barrier (whose height is about 2.2 MeV). Figure 10(b) shows the comparison between the calculated DWBA differential cross section as a function of the center-of-mass angle and the known experimental data on the $^{14}N(d,n)^{15}O_{g.s.}$ reaction at an energy of 2.4 MeV. A spectroscopic factor for the $^{14}N(d,n)^{15}O_{g.s.}$ reaction of 1.1. has been extracted. This value is in good agreement with previous results of (d,n) reactions [10] and (d,p) reactions [17] and with $1p$ shell-model calculations [18,19], as shown in Table II.

2. The $^{13}C(d,n)^{14}N^*$ (2.31 MeV) reaction

The cross section for the isospin-analog reaction to the $^{13}N(d,n)^{14}O_{g.s.}$ reaction, namely, the $^{13}C(d,n)^{14}N^*$(2.31 MeV) reaction, has been calculated using the same potential parameter set as those used for the $^{14}N(d,n)^{15}O$ calculations. Total and differential cross-section calculations have also been compared with experimental data. Three experimental cross sections have been found in the literature, at center-of-mass (c.m.) energies of 3.4 MeV [20], 4.8 MeV [11], and 10.2 MeV [21]. As an example, in Fig. 10(a), the calculated DWBA differential cross section, together with the experimental data on the $^{13}C(d,n)^{14}N^*$(2.3 MeV) reaction at a c.m. energy of 4.8 MeV, are presented. This example and the other comparisons between experiment and calculation on this reaction again show that the DWBA calculations reproduce fairly well, not only the total cross section, but also the shape of the experimental differential cross sections. The spectroscopic factor obtained for this reaction is 1.0, which is in good agreement with the results of Bobbitt, Etten, and Lenz [11] ($S=0.97$) (Table II).

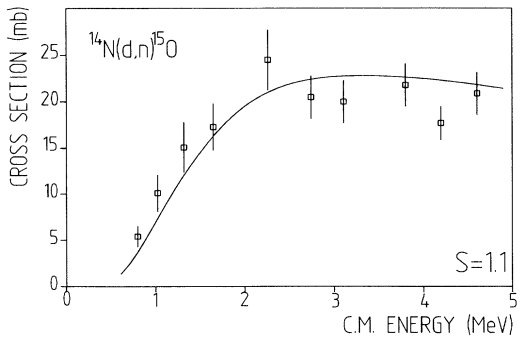

FIG. 9. Experimental excitation function [16] and DWBA calculation (with $S=1.1$) for the $^{14}N(d,n)^{15}O_{g.s.}$ reaction.

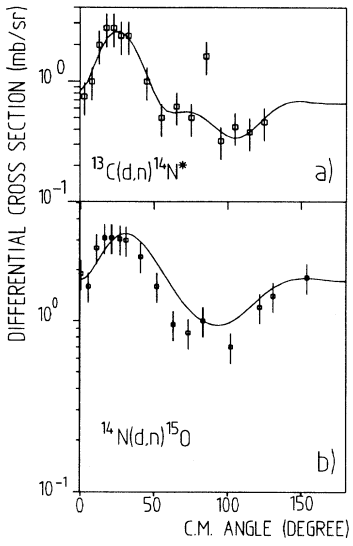

FIG. 10. Comparison between DWBA calculated and experimental differential cross sections for (a) the $^{13}C(d,n)^{14}N^*$(2.31 MeV) reaction [11] and (b) the $^{14}N(d,n)^{15}O_{g.s.}$ reaction [10].

TABLE II. Comparison between the spectroscopic factors from experimental reaction data and from theoretical shell-model calculations, for various stripping reactions.

Reaction	Present	Previous	Theory a	Theory b
$^{14}N(d,n)^{15}O_{g.s.}$	1.1	1.1[c]	1.42	1.43
$^{14}N(d,p)^{15}N_{g.s.}$		1.23[d]		
$^{13}C(d,n)^{14}N^*$ (2.3 MeV)	1.0	0.97[e]	1.39	1.73
$^{13}N(d,n)^{14}O_{g.s.}$	0.9			
$^{13}C(d,p)^{14}C_{g.s.}$		2.05[d]		

[a]Reference [19].
[b]Reference [18].
[c]Reference [10].
[d]Reference [17].
[e]Reference [11].

3. The $^{13}N(d,n)^{14}O$ reaction

The $^{13}N(d,n)^{14}O_{g.s.}$ excitation function has been calculated in the same way as the previous two reactions. The result of the DWBA calculation for the $^{13}N(d,n)^{14}O_{g.s.}$ reaction, together with the experimental data points, are shown in Fig. 11. The error bars on the data points contain the statistical uncertainty and the uncertainty on the detection efficiency at a γ ray energy of 2.3 MeV. A spectroscopic factor of 0.9 is thereby obtained. This result is in good agreement with the values extracted in (b) for the isospin analog reaction $^{13}C(d,n)^{14}N^*(2.31$ MeV), i.e., 1.0, but differs from the value extracted for the $^{13}C(d,p)^{14}C_{g.s.}$ reaction [17], i.e., 2.05 (Table II), which is also the isospin analog of the $^{13}N(d,n)^{14}O_{g.s.}$ reaction.

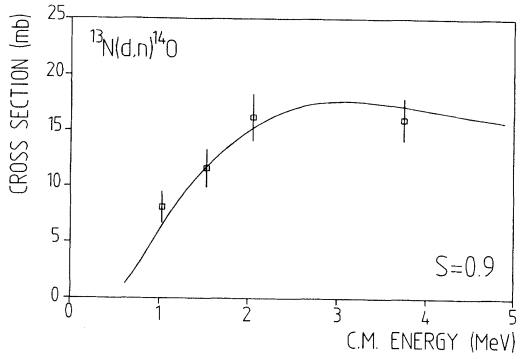

FIG. 11. Experimental excitation function and DWBA calculation (with $S=0.9$) for the $^{13}N(d,n)^{14}O_{g.s.}$ reaction.

IV. CALCULATION OF THE THERMALLY AVERAGED REACTION YIELD FOR THE $^{13}N(p,\gamma)^{14}O$ REACTION

In this section, we report on the calculation of the radiative capture cross section for the $^{13}N(p,\gamma)^{14}O$ reaction in the energy range of interest of nuclear astrophysics. Since the availability of high-intensity radioactive ^{13}N beams [4], different experiments have been performed enabling the experimental extraction of nuclear properties related to the $^{13}N(p,\gamma)^{14}O$ reaction cross section. A complete set of experimental information has been obtained in three experiments: (i) the direct measurement of the integrated cross section, between 414 and 586 keV, for the $^{13}N(p,\gamma)^{14}O$ reaction [1], which, in this energy range, is completely dominated by the $l_p=0$ resonance around 545 keV (1^- first excited state of ^{14}O at 5.17 MeV). This experiment yielded the partial γ width Γ_γ for this resonance; (ii) the determination of the resonance energy E_R and the total resonance width Γ out of the proton recoil spectra [6]; (iii) the extraction of the spectroscopic factor from the corresponding transfer reaction $^{13}N(d,n)^{14}O_{g.s.}$ in order to calculate the $^{13}N(p,\gamma)^{14}O$ reaction cross section (present paper). The obtained resonance parameters (E_R,Γ,Γ_γ) [6,22] are compared in Table III with the results from nuclear-spectroscopy [23–26] and Coulomb-breakup experiments [27,28]. A good agreement for the total and γ width between the different experimental results is observed and weighted-average values of 37.3 (0.9) keV and 3.0 (0.9) eV, respectively, are extracted. These average values have been adopted for the $^{13}N(p,\gamma)^{14}O$ astrophysical S factor calculation. The $^{13}N(p,\gamma)^{14}O$ cross section is then used to calculate the thermally averaged reaction yield in the temperature range $T=5.0\times10^7$ to 1.0×10^{10} K. As shown in Table III, the resonance energy E_R, obtained out of elastic-scattering experiments, deviates significantly from previous transfer-reaction measurements. The effect on the reaction rate of this smaller value (526 keV) compared to the higher values (540.5 and 545 keV), obtained from transfer reactions, is discussed.

A. Calculation method

The calculation of the $^{13}N(p,\gamma)^{14}O$ cross section has been performed using the formalism described by Rolfs and co-workers [2] and especially for the $^{13}N(p,\gamma)^{14}O$ reaction by Fernandez, Adelberger, and Garcia [24]. The total capture cross section is expressed as follows:

$$\sigma(E)=\sigma_r(E)+\sigma_{nr}(E)+2[\sigma_r(E)\sigma_{nr}(E)]^{1/2}\cos[\delta_r(E)] \quad (8)$$

TABLE III. Summary of the resonance energy E_R, the total width Γ, and the partial γ width Γ_γ for the $^{13}N(p,\gamma)^{14}O$ resonant reaction (1^- first excited state in ^{14}O) as obtained from different experimental data.

Experiment	E_R (keV)	Γ (keV)	Γ_γ (eV)	Ref.
$^1H(^{13}N,\gamma)^{14}O$			3.3 $(0.7)_{stat}(0.6)_{syst}$	[22]
$^1H(^{13}N,^1H)^{13}N$	526.0 (1.0)	37.0 (1.1)		[6]
$^{12}C(^3He,n)^{14}O$	545 (10)		2.7 (1.3)	[23]
$^{12}C(^3He,n)^{14}O$			7.6 (3.8)	[24]
$^{12}C(^3He,n)^{14}O$			<17	[25]
$^{14}N(^3He,t)^{14}O$	540.5 (1.8)	38.1 (1.8)	3.1 (0.6)	[26]
$^{208}Pb(^{14}O,^{13}N\ p)^{208}Pb$			2.4 (0.9)	[27]
$^{208}Pb(^{14}O,^{13}N\ p)^{208}Pb$			3.0 (0.4)	[28]
	529.4 (0.9)	37.3 (0.9)		a

[a]Weighted-average values.

The resonance contribution $\sigma_r(E)$ is given by the Breit-Wigner parametrization:

$$\sigma_r(E)=\frac{(\omega\lambda^2/4\pi)\Gamma_p(E)\Gamma_\gamma(E)}{\{(E-E_r)^2+[\Gamma_{\rm tot}(E)/2]^2\}} , \quad (9)$$

which depends on the gamma width $\Gamma_\gamma(E)$, the proton width $\Gamma_p(E)$, and the total width $\Gamma_{\rm tot}(E)$ $[\approx\Gamma_p(E)]$. The energy dependence of these widths can be expressed as follows [3]:

$$\Gamma_\gamma(E)=\frac{\Gamma_\gamma(E_R)(Q+E)^{2l+1}}{(Q+E_R)^{2l+1}} ,$$
$$\Gamma_p(E)=\frac{\Gamma_p(E_R)\exp[-(E_G/E)^{1/2}]}{\exp[-(E_G/E_R)^{1/2}]} . \quad (10)$$

The quantity l is the multipolarity of the gamma transition which, in the case of $^{13}N(p,\gamma)^{14}O$, is dominated by a $l=1(E1)$ transition; E_R is the resonance energy; Q is the reaction Q value; E_G is the Gamow energy. The statistical factor ω in Eq. (9) is equal to

$$(2J+1)/[(2J_1+1)(2J_2+1)] ,$$

where J_1, J_2, and J are the spins of the projectile, of the target atoms, and of the resonant level, respectively. The nonresonant contribution $\sigma_{\rm nr}(E)$ is given by [2,5]

$$\sigma_{\rm nr}=\sum_{lsj} C^2S_{lj}|T^{\rm DC}_{slj}|^2 \quad (11)$$

where C, S_{lj}, and $T^{\rm DC}_{slj}$ are the isospin Clebsh-Gordan coefficient, the spectroscopic factor, and the direct-capture transition amplitude, respectively. The nonresonant cross section for the $E1$ transition has been calculated using the direct-capture program TEDCA [29]. For the entrance channel, hard-sphere nuclear phase shifts have been used (hard sphere potential with a radius $R=3.7$ fm); the final bound state is calculated using a folding potential.

The resonant phase $\delta_r(E)$ in the third term of Eq. (8), which describes the interference between resonant and nonresonant capture, is given by [2]

$$\delta_r(E)=\tan^{-1}[\Gamma(E)/2(E-E_r)] . \quad (12)$$

In addition to the cross section, one can also calculate the astrophysical S factor, which is defined as follows [3]:

$$S(E)=\sigma(E)E\exp(E_G/E)^{1/2} . \quad (13)$$

Using this S factor, the thermally averaged reaction yield, expressed in units of $\rm cm^3\,s^{-1}\,mole^{-1}$, is given by the following expression [30]:

$$N_A\langle\sigma V\rangle=3.873\times10^{10}T_g^{-3/2}\int S(E)\exp[-(E_G/E)^{1/2}-11.605E/T_9]dE , \quad (14)$$

where T_9 is the temperature in units of 10^9 K.

B. Results

In order to check the validity of the calculation, the astrophysical S factor for the $^{13}C(p,\gamma)^{14}N^*(2.31$ MeV) reaction, which is the isospin analog of the $^{13}N(p,\gamma)^{14}O_{g.s.}$ reaction, has been calculated, using the experimental resonance parameters [6,31] and a spectroscopic factor of 1.0 obtained from the $^{13}C(d,n)^{14}N$ reaction (see Table II). The results of this calculation is plotted in Fig. 12 together with the S factor deduced from experimental cross-section data [31]. The comparison clearly shows a positive interference effect below and a destructive interference effect above the resonance energy. A good agreement between theory and experiment is observed.

Figure 13 shows the astrophysical S factor calculation of the $^{13}N(p,\gamma)^{14}O$ reaction. For the nonresonant calculation, the experimental spectroscopic factor of 0.9, obtained in the present work for the $^{13}N(d,n)^{14}O_{g.s.}$ reaction, has been used. The calculated nonresonant S factor can be reproduced by the following analytical function, which makes further calculations easier:

$$S_{\rm nr}=C^2S3.44\times10^{-4}\exp[-0.605E({\rm MeV})] \ ({\rm MeV\,b}) . \quad (15)$$

Figure 13 shows that the $^{13}N(p,\gamma)^{14}O$ reaction cross section is strongly dominated by the resonance at 526 keV; the effect of the nonresonant contribution, or the deviation from a pure Breit-Wigner form (9), is only seen below and above the resonance by constructive and destructive interference effects, respectively. At an energy of about 100 keV, this interference effect increases the S factor by about 100% as compared with a pure Breit-Wigner resonant S factor. It is clear that the interference effect is less important in the $^{13}N(p,\gamma)^{14}O$ reaction as compared with the $^{13}C(p,\gamma)^{14}N^*(2.31$ MeV) reaction (Fig. 12). The $^{13}N(p,\gamma)^{14}O$ astrophysical S factor result is quite consistent with the calculation of Fernandez,

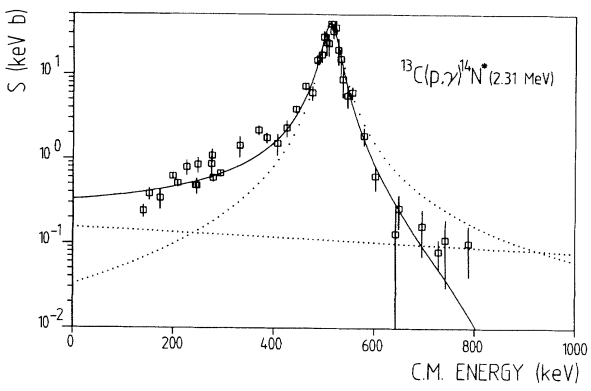

FIG. 12. Comparison between the experimental astrophysical S factor for the $^{13}C(p,\gamma)^{14}N^*(2.31$ MeV) reaction [31] and the calculations; the resonant and the nonresonant contributions are plotted separately (dotted lines).

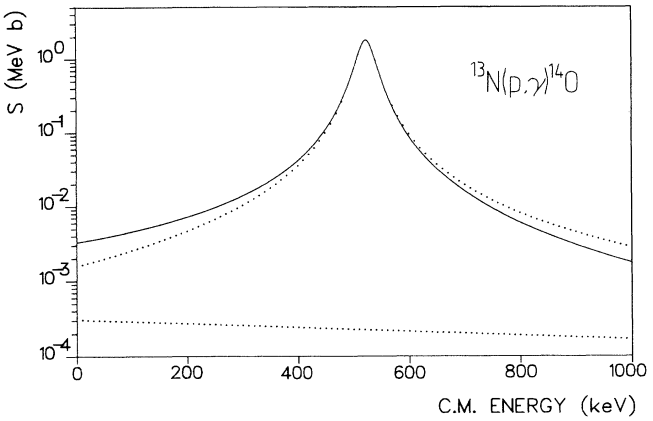

FIG. 13. Calculation of the total astrophysical S factor of the $^{13}N(p,\gamma)^{14}O_{g.s.}$ reaction; the resonant and nonresonant contributions are plotted separately (dotted lines).

Adelberger, and Garcia [24] where Γ_γ and Γ values of 2.7 eV and 38.1 keV, respectively, were adopted and where the nonresonant contribution was deduced using the spectroscopic factor of the analog state in ^{14}N.

In Table IV the thermally averaged reaction rate for the $^{13}N(p,\gamma)^{14}O$ reaction, calculated with Eq. (14), is compared with the compilation values of Caughlan and Fowler [32], showing a presently larger reaction rate over the entire energy range. In addition, the thermally averaged reaction rate, calculated by taking only into account the pure Breit-Wigner resonant S factor, is also given in Table III: for low temperatures ($T \leq 1.0\times10^8$ K), the total S factor is about a factor of 2 larger than the resonant contribution only; for very high temperatures ($T \geq 2.0\times10^9$ K), the total reaction rate can become smaller than the resonant contribution only. This is simply a consequence of the above-mentioned difference between the total S factor and the pure resonant S factor.

Besides using 526 keV as resonance energy, the reaction rate has also been calculated using the 545 keV value. The results in Table IV show that the effect of using a lower resonance energy is an increase of the reaction rate with 17–32 %, depending on the temperature.

V. SUMMARY

A calculation of the $^{13}N(p,\gamma)^{14}O_{g.s.}$ astrophysical S factor, based on the experimental nuclear physics information, has been performed including a resonant (Breit-Wigner) and a nonresonant contribution. As a good agreement exists between the results from our direct measurements with ^{13}N beams and the results from nuclear spectroscopy and Coulomb-breakup experiments, mean-average values for the total and γ width have been adopted. Using this S factor, the thermally averaged reaction rate is calculated and the effect of the resonance energy

TABLE IV. The $^{13}N(p,\gamma)^{14}O$ reaction rate as a function of temperature. See text for the definition of the symbols used.

	$N_A\langle\sigma v\rangle$ ($cm^3 s^{-1} mole^{-1}$)			
	Caughlan and Fowler[a]	Present		
$T(10^9$ K)		$E_R=545$ keV	$E_R=526$ keV	b
0.05	3.57×10^{-10}	4.62×10^{-10}	5.54×10^{-10}	2.94×10^{-10}
0.06	3.66×10^{-9}	4.78×10^{-9}	5.75×10^{-9}	3.09×10^{-9}
0.07	2.35×10^{-8}	3.11×10^{-8}	3.74×10^{-8}	2.04×10^{-8}
0.08	1.09×10^{-7}	1.46×10^{-7}	1.76×10^{-7}	9.70×10^{-8}
0.09	4.01×10^{-7}	5.38×10^{-7}	6.52×10^{-7}	3.63×10^{-7}
0.1	1.23×10^{-6}	1.66×10^{-6}	2.02×10^{-6}	1.14×10^{-6}
0.2	8.62×10^{-4}	1.19×10^{-3}	1.48×10^{-3}	9.30×10^{-4}
0.3	2.35×10^{-2}	3.65×10^{-2}	4.85×10^{-2}	3.47×10^{-2}
0.4	3.07×10^{-1}	5.46×10^{-1}	8.00×10^{-1}	6.90×10^{-1}
0.5	2.93	4.98	7.24	6.75
0.6	15.9	25.2	35.2	33.7
0.7	54.1	82.1	110	107
0.8	135	198	256	251
0.9	269	388	490	483
1.0	463	658	812	803
2.0	3.77×10^{-3}	5.39×10^{3}	601	607
3.0	5.67×10^{3}	8.58×10^{3}	926	947
4.0	6.21×10^{3}	9.63×10^{3}	10.2×10^{3}	10.6×10^{3}
5.0	6.11×10^{3}	9.63×10^{3}	10.1×10^{3}	10.6×10^{3}
6.0	5.74×10^{3}	9.19×10^{3}	9.60×10^{3}	10.1×10^{3}
7.0	5.30×10^{3}	8.60×10^{3}	8.96×10^{3}	9.52×10^{3}
8.0	4.86×10^{3}	7.99×10^{3}	8.30×10^{3}	8.88×10^{3}
9.0	4.45×10^{3}	7.41×10^{3}	7.68×10^{3}	8.28×10^{3}
10.0	4.07×10^{3}	6.88×10^{3}	7.12×10^{3}	7.71×10^{3}

[a]Reference [32].
[b]Calculation using resonant contribution only and $E_R=526$ keV.

on the accuracy of the rate has been discussed.

The spectroscopic factor, necessary for calculating the nonresonant contribution, is obtained by studying the $^{13}N(d,n)^{14}O_{g.s.}$ reaction. The possibility of measuring cross sections for stripping reactions where short-living nuclei are involved was made possible in reverse kinematics by using high-intensity radioactive ^{13}N beams and $(CD_2)_n$ target foils. Accelerated radioactive beams of 8.2 MeV ($^{13}N^{1+}$), 12.0, 16.2, and 28.5 MeV ($^{13}N^{2+}$) have been used. The comparison between the experimental $^{13}N(d,n)^{14}O_{g.s.}$ excitation curve and the results of a DWBA calculation (obtained after an investigation of analog stripping reactions) allowed to extract a spectroscopic factor of 0.9. In this way, we have obtained a rather complete understanding of the astrophysically important proton capture reaction on ^{13}N.

ACKNOWLEDGMENTS

We would like to thank the crew of the Louvain-la-Neuve cyclotrons for delivering the excellent radioactive beams and P. Demaret for making the good quality $(CD_2)_n$ foils. Thanks also to K. Gruen and H. Krauss for their help in working with the DWBA and direct-capture codes. This text presents research results of the Belgian Programme on Interuniversity Poles of Attraction, initiated by the Belgian State, Prime Minister's Office, Science Policy Programming. We also want to acknowledge the "Fonds zur Foerderung der Wissenschaftlichen Forschung in Oesterreich," project No. P7838-TEC. G. V. and P. Le. acknowledge the National Fund for Scientific Research (Belgium), and M. G. the Belgian "I.W.O.N.L."

[1] P. Decrock, Th. Delbar, P. Duhamel, W. Galster, M. Huyse, P. Leleux, I. Licot, E. Lienard, P. Lipnik, M. Loiselet, C. Michotte, G. Ryckewaert, P. Van Duppen, J. Vanhorenbeeck, and J. Vervier, Phys. Rev. Lett. **67**, 808 (1991).

[2] C. Rolfs, Nucl. Phys. **A217**, 29 (1973); C. Rolfs and R. E. Azuma, *ibid.* **A227**, 291 (1974); C. Rolfs and W. S. Rodney, *ibid.* **A235**, 450 (1974).

[3] C. Rolfs and W. S. Rodney, *Cauldrons in the Cosmos* (University of Chicago Press, Chicago, 1988).

[4] D. Darquennes, P. Decrock, Th. Delbar, W. Galster, M. Huyse, Y. Jongen, M. Lacroix, P. Leleux, I. Licot, E. Lienard, P. Lipnik, M. Loiselet, G. Ryckewaert, S. Wa Kitwanga, P. Van Duppen, J. Vanhorenbeeck, J. Viervier, and S. Zaremba, Phys. Rev. C **42**, R804 (1990).

[5] H. Oberhummer, in *Nuclei in the Cosmos,* edited by H. Oberhummer (Springer Verlag, Berlin, 1991), p. 29.

[6] Th. Delbar, W. Galster, P. Leleux, E. Lienard, P. Lipnik, C. Michotte, J. Vervier, P. Duhamel, J. Vanhorenbeeck, P. Decrock, M. Huyse, P. Van Duppen, D. Baye, and P. Descouvement, Nucl. Phys. **A542**, 263 (1992).

[7] F. Ziegler, *The Stopping and Ranges of Ions in Matter* (Pergamon, New York, 1980), Vol. 5.

[8] L. C. Northcliffe and R. F. Schilling, Nucl. Data Tables A **7**, 233 (1970).

[9] R. H. Siemssen, M. Cosack, and R. Felst, Nucl. Phys. **69**, 209 (1963); **69**, 227 (1963).

[10] R. C. Ritter, E. Sheldon, and M. Strang, Nucl. Phys. **A140**, 609 (1970).

[11] J. R. Bobbitt, M. P. Etten, and G. H. Lenz, Nucl. Phys. **A203**, 353 (1973).

[12] K. Gruen, Technical University, Wien, Computer code FREDICA, 1990 (unpublished); K. Gruen, Ph.D thesis, 1992 (unpublished).

[13] H. De Vries, C. W. De Jager, and C. De Vries, At. Data Nucl. Data Tables **36**, 495 (1987).

[14] A. M. Kobos, B. A. Brown, R. Lindsay, and G. R. Satchler, Nucl. Phys. **A425**, 205 (1984).

[15] C. M. Perey and F. G. Perey, At. Data Nucl. Data Tables **17**, 1 (1976).

[16] Th. Retz-Schmidt and J. L. Weil, Phys. Rev. **3**, 119 (1960).

[17] J. P. Schiffer, G. C. Morrison, R. H. Siemssen, and B. Zeidman, Phys. Rev. **164**, 1274 (1967).

[18] S. Cohen and D. Kurath, Nucl. Phys. **A101**, 1 (1967).

[19] S. Varma and P. Goldhammer, Nucl. Phys. **A125**, 193 (1969).

[20] R. E. Benenson and B. Yaramis, Phys. Rev. **129**, 720 (1963).

[21] G. S. Mutchler, D. Rendic, D. E. Velkley, W. E. Sweeney, and G. C. Phillips, Nucl. Phys. **A172**, 469 (1971).

[22] P. Decrock, Th. Delbar, P. Duhamel, W. Galster, M. Huyse, P. Leleux, I. Licot, E. Lienard, P. Lipnik, C. Michotte, P. Van Duppen, J. Vanhorenbeeck, and J. Vervier, Phys. Lett. B **304**, 50 (1993).

[23] M. B. Greenfield and C. R. Bingham, Phys. Rev. C **6**, 1756 (1972).

[24] P. B. Fernandez, E. G. Adelberger, and A. Garcia, Phys. Rev. C **40**, 1887 (1989)

[25] P. Aguer, G. Bogaert, M. Kious, V. Landré, A. Lefebvre, J. B. Thibaud, F. Beck, and A. Huck, in *Proceedings of the International Symposium on Heavy Ion Physics and Nuclear Astrophysical Problems,* Tokyo, Japan, 1988, edited by S. Kubono, M. Ishihara, and T. Nomura (World Scientific, Singapore, 1989), p. 107.

[26] T. E. Chupp, R. T. Kouzes, A. B. McDonald, P. D. Parker, T. F. Wang, and A. Howard, Phys. Rev. C **31**, 1023 (1985).

[27] T. Motobayashi, T. Takei, S. Kox, C. Perrin, F. Merchez, D. Rebreyend, K. Ieke, H. Murakami, Y. Ando, N. Iwasa, M. Kurakowa, S. Shirato, J. Ruan, T. Ichihara, T. Kubo, N. Inabe, A. Goto, S. Kubono, S. Shimoura, and M. Ishihara, Phys. Rev. B **264**, 259 (1991).

[28] J. Kiener, A. Lefebvre, P. Aguer, C. O. Bacri, R. Bimbot, G. Bogaert, B. Borderie, F. Clapier, A. Coc, D. Disdier, S. Fortier, C. Grinberg, L. Kraus, I. Linck, G. Pasquier, M. F. Rivet, F. St. Laurent, C. Stephan, L. Tassan-Got, and J. P. Thibaud, Nucl. Phys. **A52**, 66 (1993).

[29] H. Krauss, Technical University, Wien, Computer code TEDCA, 1991 (unpublished); H. Krauss, Ph.D. thesis, 1992 (unpublished).

[30] W. A. Fowler, G. R. Caughlan, and B. A. Zimmerman, Annu. Rev. Astron. Astrophys. **5**, 525 (1967).

[31] R. E. Azuma, J. D. King, J. B. Vise, J. Goerres, H. P. Trauvetter, C. Rolfs, and A. E. Vlieks, in *Proceedings of the Accelerated Radioactive Beams Workshop,* edited by L. Buchmann and J. M. D'Auria (TRIUMF, Vancouver, Canada, 1985), p. 70; R. E. Azuma, J. D King, J. B. Vise, J. Goerres, C. Rolfs, H. P. Trauvetter, and A. E. Vlieks (unpublished).

[32] G. R. Caughlan and W. A. Fowler, At. Data Nucl. Data Tables **40**, 283 (1988).